Renewable and Sustainable Energy Reviews 32 (2014) 684–696

Contents lists available at ScienceDirect

Renewable and Sustainable Energy Reviews

journal homepage: www.elsevier.com/locate/rser

A comparison of different one-diode models for the representation of *I–V* characteristic of a PV cell

Giuseppina Ciulla*, Valerio Lo Brano, Vincenzo Di Dio, Giovanni Cipriani

DEIM Dipartimento di Energia, Ingegneria dell'Informazione e Modelli Matematici, Università degli studi di Palermo, Edificio 9, viale delle scienze, Palermo, Italy

ARTICLE INFO

Article history:
Received 3 April 2013
Received in revised form
19 December 2013
Accepted 4 January 2014
Available online 8 February 2014

Keywords:
Five parameter model
I–V characteristic
PV cell
Renewable energy

ABSTRACT

Predictive performance tools are an important factor in the success of any new technology because they permit demonstration of whether a system will be efficient and economically feasible. A reliable predictive tool should allow the designer to optimise system performance and to maximise the cost effectiveness of a system prior to installation. This article discusses the five main parametric models for photovoltaic (PV) systems available in the literature. The current–voltage characteristics of a photovoltaic module can be reproduced modelling the PV panel as an equivalent electrical circuit made of linear and non-linear components. The parameters describing such components are directly related to the performance characteristics of the specific PV panel, which are generally available in a graphic form with respect to standard values of temperature and incident irradiance. Five of the most recent models are analysed in detail describing the algorithm, showing how the parameters were determined and highlighting the most important mathematical and physical assumptions that characterised each model and the calculation process. To simplify the examination and reading of the procedures referred to in the five models, all equations are rewritten using the same nomenclature. Furthermore, to assess the accuracy of each model with respect to the data provided by the manufacturer, this paper compares the *I–V* and *P–V* curves at various temperatures and irradiance for a generic PV panel.

Contents

1. Introduction . . . 685
2. Solar photovoltaic technologies . . . 685
3. Generic electric behaviour of a solid single junction PV cell . . . 686
   3.1. De Blas, Torres, Pieto and Garcìa model . . . 688
      3.1.1. Mathematical and physical assumptions . . . 689
      3.1.2. The algorithm steps . . . 689
   3.2. Hadj Arab, Chenlo and Benghanem model . . . 689
      3.2.1. Mathematical and physical assumptions . . . 690
      3.2.2. The algorithm steps . . . 690
   3.3. De Soto, Klein and Beckman model . . . 690
      3.3.1. Mathematical and physical assumptions . . . 691
      3.3.2. The algorithm steps . . . 691
   3.4. Villalva, Gazoli and Filho model . . . 691
      3.4.1. Mathematical and physical assumptions . . . 691
      3.4.2. The algorithm steps . . . 692
   3.5. Lo Brano, Orioli, Ciulla and Di Gangi model . . . 692
      3.5.1. Mathematical and physical assumptions . . . 692
      3.5.2. The algorithm steps . . . 692
4. Discussion . . . 693
   4.1. Availability of necessary input data . . . 693

* Corresponding author. Tel.: +39 091 238 619 18; fax: +39 091 484 425.
E-mail address: ina@dream.unipa.it (G. Ciulla).

1364-0321/$ - see front matter © 2014 Elsevier Ltd. All rights reserved.
http://dx.doi.org/10.1016/j.rser.2014.01.027

4.2. Synopsis of the major hypothesis and simplifications . . . 693
4.3. Numerical performance . . . 693
4.4. Overview of the models, hypothesis and simplifications . . . 695
5. Concluding remarks . . . 695
References . . . 696

1. Introduction

A steady increase in hydropower and the rapid expansion of wind and solar power has cemented the position of renewables as an indispensable part of the global energy mix; by 2035, renewables will account for almost one-third of the total electricity output. Solar power is growing more rapidly than any other renewable technology. Renewables will become the world's second-largest source of power generation by 2015 (roughly half that of coal), and, by 2035, they will rival coal as the primary source of global electricity [1].

In this framework, photovoltaic generation systems have the opportunity to be suitable for use due to their important advantage in being able to produce electrical energy very close to the electric load. In this way, transmission losses are avoided, and it is also possible to satisfy the peaks in the daily load diagrams because they supply the maximum power in correspondence to the maximum request. Moreover, photovoltaic plants do not emit pollutant emissions or vibrate; due to their modularity, they can comply with the morphology of the installation sites [2].

Promoting the dissemination of renewable energy sources is essential for accurate assessment of power production to estimate the economic and environmental performance with a high grade of reliability [3,4].

In the field of PV systems, it is essential to have a good simulation tool that can forecast the physical behaviour of a PV panel by varying the solar irradiance and the operating temperature. The operating temperature is also a key variable of the forecasting problem because it directly affects the electrical outputs (current, voltage and power) and the efficiency of the solar device. One of the thermo-physical processes that most affects the value of the operating temperature is represented by convective and radiative heat exchange between the panel and the surrounding environment. In [5], it was observed that the convective heat transfer coefficient is strongly influenced by the wind speed, although it is less affected by the wind direction and is almost unaffected by the air temperature. Concerning the radiative heat exchange, the operating temperature also strongly depends on the glass transparency and the emissivity and absorption coefficient of the cell. Some authors have attempted to estimate the operating regimen of a photovoltaic panel connected to an electrical load in a simple and precise model, noting the operating temperature [6–8].

Some existing software, such as PVFORM [9,10], PVWATTS [11], PHANTASM [12], TRNSYS [13] and PVsyst [14], which is quite sophisticated and is intended for advanced users, evaluates the physical behaviour of a photovoltaic component and requires a large number of parameters, which are difficult to find in technical data and which are often published without the correlations used. Consequently, normal users usually employ the databases included, sometimes without understanding the importance of these data in the assessment of the power output. For these reasons, it is certainly wise to learn more about the features and the mathematical approximations of the various models used to describe the thermo-electrical behaviour of PV systems.

The algorithms and models that can be used to assess the PV power output are generally of two types: those that use selected points of the *I–V* curve [15–19] and those that exploit the entire characteristic curve [20–23]. The first group of algorithms involves the solution of five equations, using thermal drift coefficients, measuring the slope of the *I–V* curve and exploiting selected points, i.e., the open-circuit, short-circuit and maximum power points. Although calculating the exact solution of these equations requires iterative techniques, this method is often much faster and simpler compared to the second group of models. Indeed, the group of algorithms based on curve fitting, using deterministic optimisation algorithms, has a disadvantage that leads to solutions for several sets of local minima [24].

Within the first group of algorithms, the analytical models that are employed the most evaluate a solar cell as an equivalent electrical circuit composed of a set of generally non-linear components. The electrical parameters of the equivalent circuit are directly related to the performance characteristics of the photovoltaic component, which are generally described in graphical form for standard values of temperature and irradiance.

The paper is organised as follows: Section 2 presents the types of PV, related topics and their performances; and Section 3 presents the equivalent circuit for PV modules and describes the five most recent and most cited mathematical models. An outline of the parameter extraction procedure is given for each model. Section 4 presents a discussion of the results obtained along with the procedures used.

2. Solar photovoltaic technologies

The photovoltaic technologies are generally divided into five categories:

1. ***Multi-junction solar cells***: Multi-junction solar cells, or tandem cells, are solar cells containing several *p–n* junctions. Each junction is tuned to a different wavelength of light, which reduces one of the largest inherent sources of losses, thereby increasing the efficiency. Traditional single-junction cells have a maximum theoretical efficiency of 34%; a theoretical "infinite-junction" cell would improve this efficiency to 87% under highly concentrated sunlight.
2. ***Single-junction GaAs***: Gallium arsenide is an important optical compound semiconductor and is a nearly ideal material for high efficiency single-junction solar cells. In addition, GaAs is capable of withstanding radiation damage for a long time. Owing to its high efficiency and high resistance to radiation, GaAs cells have been favourites for powering satellites and other spacecraft [25].
3. ***Crystalline Si cells***: Silicon technology has been the dominant one for supplying power modules in photovoltaic applications, and the changes likely are an increasing proportion of multi-crystalline silicon and mono-crystalline silicon being used for high-efficiency solar cells, while the use of thinner wafers and ribbon silicon technology continues to grow [26,27].
4. ***Thin-film technologies***: Thin-film solar cells are basically thin layers of semiconductor materials applied to a solid backing material. Thin films greatly reduce the amount of semiconductor material required for each cell compared to silicon wafers, and hence, lower the cost of production of photovoltaic cells.

Nomenclature

a	ideality factor
D	diode diffusion factor (approximately constant)
G	irradiance [W/m^2]
G_{SRC}	irradiance at SRC [W/m^2]
I	current generated by the panel [A]
I_D	diode current [A]
I_L	photocurrent [A]
I_{mp}	current at the maximum power point [A]
I_{SC}	short circuit current of the panel [A]
I_0	reverse saturation current [A]
K	thermal correction factor [Ω/°C]
k	Boltzmann constant [1.381×10^{-23} J/K]
J	thermal correction factor
M	air mass
m	constant
n	diode quality factor
N_s	number of cells wired in series
q	electron charge [1.602×10^-19 C]
R_L	electrical load [Ω]
R_s	series resistance [Ω]
R_{s0}	reciprocal of slope of the I–V characteristic of the panel for $V = V_{OC}$ [V] and $I = 0$ [Ω]
R_{sh}	shunt resistance [Ω]
R_{sh0}	reciprocal of the slope of the I–V characteristic of the panel for $V = V_{OC}$ [V] and $I = 0$ [Ω]
SRC	Standard Reference Conditions
T	cell temperature of the PV panel [K]
V	voltage generated by the PV panel [V]
V_{mp}	voltage at the maximum power point [V]
V_{OC}	open circuit voltage of the panel [V]

Greek symbols

α	ratio between the current irradiance and the irradiance at SRC
ε_{ref}	material band-gap energy [1.12 eV for silicon]
ε_{SRC}	amplitude of energy gap [J]
γ	shape factor
$\mu_{I,sc}$	thermal coefficient of the short circuit current [A/°C]
$\mu_{V,oc}$	thermal coefficient of the open circuit voltage [V/°C]

GaAs, copper, cadmium telluride (CdTe), indium diselenide ($CuInSe_2$) and titanium dioxide (TiO_2) are materials that have been used the most for thin-film PV cells [27].

5. ***Other emerging photovoltaic***: In this category, there are different types of PV technology, such as dye-sensitised, organic, inorganic and quantum dot solar cells.

A *dye-sensitised solar cell* (DSSC, DSC or DYSC) is a low-cost solar cell belonging to the group of thin-f0ilm solar cells [28]. It is based on a semiconductor formed between a photo-sensitised anode and an electrolyte that constitutes a photo-electrochemical system.

Organic photovoltaic (OPV or excitonic) cells may be based on organic dyes, semiconducting polymers, small semiconductor molecules, or on some combination of these species. In all cases, however, light absorption by the organic species primarily results in the production of excitons rather than free electron–hole pairs [29]. These cells are cheaper to produce, lighter and more flexible than traditional silicon-based solar cells, and therefore, have a wider range of applications.

Inorganic cells: In thin-film technologies, there exists a common problem with conversion efficiency due to poor material quality; photo-generated electrons and holes cannot travel very far before recombination (short free-carrier diffusion lengths). If a solar cell can be made using nanoscale hetero-junctions, then each photo-generated carrier will have less distance to travel, and the problem of recombination can be greatly reduced. The main factor for the superior efficiency of inorganic devices over organic devices lies in the high intrinsic carrier mobilities that exist in inorganic semiconductors. Higher carrier mobility means that charges are transported to the electrodes more quickly, which reduces current losses via recombination [30].

Quantum dot solar cells (QDSCs) are based on the Gratzel cell, or dye-sensitised solar cell, architecture but employ low band gap semiconductor nanoparticles that possess such small crystallite sizes that they form quantum dots (such as CdS, CdSe, Sb_2S_3 and PbS), instead of organic or organometallic dyes, as light absorbers. A quantum dot is a portion of matter that has electronic properties that are intermediate between those of bulk semiconductors and those of discrete molecules [31].

In general, silicon wafer-based photovoltaic cells that include single crystal, multi-crystalline and the hetero-structure have more than 80% of the market share [32]. The record conversion efficiency of a multi-crystalline photovoltaic cell is 20.4%, while a single crystal silicon cell can reach an efficiency of 26.4% (Table 1).

To evaluate the performance and price of different PV module technologies above summarised, we can refer to the studies conducted by the International Energy Agency (IEA) exemplified in Fig. 1 [33], or in more recent studies [27].

The record conversion efficiency of amorphous silicon cells is 13.4%, while the record efficiencies of CdTe and $CuInSe_2$ are 18.7% and 20.4%, respectively. Microcrystalline silicon has experienced a breakthrough recently and has reached an efficiency close to that of CdTe. Third-generation photovoltaic cells are solar cells that are potentially able to overcome the Shockley-Queisser limit of 31–41% power efficiency for single band-gap solar cells. Common third-generation systems include multi-layer cells made of amorphous silicon or gallium arsenide, whereas more theoretical developments include frequency conversion, hot-carrier effects and other multiple-carrier ejection. Third-generation photovoltaic cell technology is still in the early development stage. The cost–benefit ratio of this technology is still too high to be competitive with the previous generation counterpart.

3. Generic electric behaviour of a solid single junction PV cell

When a solid single junction PV cell is not illuminated, its behaviour is similar to a semiconductor junction; a simple diode, which has a characteristic I–V curve, is traditionally described by the equation:

$$I_D = I_0\left(e^{\frac{qV_D}{nkT}} - 1\right) \tag{1}$$

where I_0 is the reverse saturation current of the diode, $q$is the electric charge of an electron (1.602×10^{-19} C), $k$is the Boltzmann constant (1.381×10^{-23} J/K), T is the junction temperature, V_D is the voltage across the diode and n is the ideality factor, also known as the quality factor or sometimes the emission coefficient. The ideality factor n typically varies from 1 to 2 (though it can be

higher in some cases), depending on the fabrication process and semiconductor material; in many cases, n is assumed to be approximately equal to 1 (thus, the notation n often is omitted).

The illumination of the semiconductor junction determines the rise of a photo-generated current I_L that determines a vertically translation of the I–V curve of a quantity linked, almost exclusively, to the surface density of the incident energy (Fig. 2).

In this way, an ideal cell is represented as a current generator, connected in parallel with a diode, and its I–V characteristic is described by Shockley [35] with the following equation:

$$I = I_L - I_D = I_L - I_0\left(e^{\frac{qV_D}{nkT}} - 1\right) \tag{2}$$

where I is the output current.

Table 1
Best research-cell efficiencies of 2013/03 [34].

Category	*Types*	*Efficiency [%]*
Multi-junction cells (2-teminal monolithic)	Four junction or more (no concentrator)	37.80
	Three junction (concentrator)	44.00
	Three junction (no concentrator)	37.70
	Two junction (concentrator)	32.60
	Two junction (no concentrator)	30.80
Single junction GaAs	Concentrator	29.10
	Thin film crystal	28.80
	Single crystal	26.40
	Single crystal	27.10
	Thin film crystal	20.10
Crystalline Si cells	Silicon heterostructures (HIT)	24.70
	Multi-crystalline	20.40
	Thick Si film	16.00
	Cu (In, Ge) Se_2	20.40
Thin film technologies	CdTe	18.70
	Nano-micro-poly-Si	17.20
	Multi-junction poly-crystalline	15
	Amorphous SiH (stabilized)	13.40
Emerging photovoltaic	Dye-sensitized cells	11.40
	Organic cells	11.10
	Inorganic cells	11.10
	Organic tandem cells	12.00
	Quantum dot cells	7.00

Eq. (2) represents only a mere theoretical description because it does not take into account the effect due to the presence of the electrodes both above and below the semiconductor layer that are necessary for collecting the charges that partially cover the intercepting surface. In [36], Wolf correctly observed that in a PV cell, the photocurrent is generated not only by a single diode but also by a global effect due to the presence of a plurality of adjacent and uniformly distributed elementary diodes along the surface that separates the two layers of the semiconductor. Each elementary diode is traversed by a current that flows across the semiconductor layers along a different line, characterised by different electric resistance and voltage drop.

The transverse component of the current I_L, parallel to the surface of the cell, should be different for each elementary diode; in this way, there is a different characteristic I–V for each elementary diode. Because these diodes are considered in parallel, the combination of them determines the global I–V characteristic of the PV cell. The transverse electrical resistance is much higher than the electrical resistance relative to the direct component of I_L. The transverse component of the current I_L, which only occurs in a real photovoltaic cell, gives rise to a high energy dissipation that drastically decreases the conversion efficiency of the solar cell.

Wolf, in [36], proposed a simplified equivalent circuit, shown in Fig. 3, in which there are only a couple of diodes, one current generator and two resistors that take account of the dissipative effects above described and of the presence of any constructive defects.

The resolution of the above equivalent circuit permits to obtain the following expression of the I current in an implicit form:

$$I = I_L - I_{01}\left(e^{\frac{V+IR_s}{n_1 T}} - 1\right) - I_{02}\left(e^{\frac{V+IR_s}{n_2 T}} - 1\right) - \frac{V+IR_s}{R_{sh}} \tag{3}$$

where I_L is proportional to the irradiance [35]; I_{01} and I_{02} are the diode saturation current of the two diodes, R_s and $R_{sh}$are the series and parallel resistances, respectively; and n_1 and n_2 are the ideality factors of the two diodes. As it is easy to see from Fig. 3, it is necessary to know seven parameters ($I_L, n_1, n_2, I_{01}, I_{02}, R_s, R_{sh}$) to solve Eq. (3).

In detail, the resistors R_{sh} and R_s alter the slope of the curve before and after the "knee" of the curve, respectively, while the ratio between I_{01} and I_{02} changes the curvature [37].

Despite not being a mathematically indeterminate problem, calculation of the seven parameters is made difficult by the

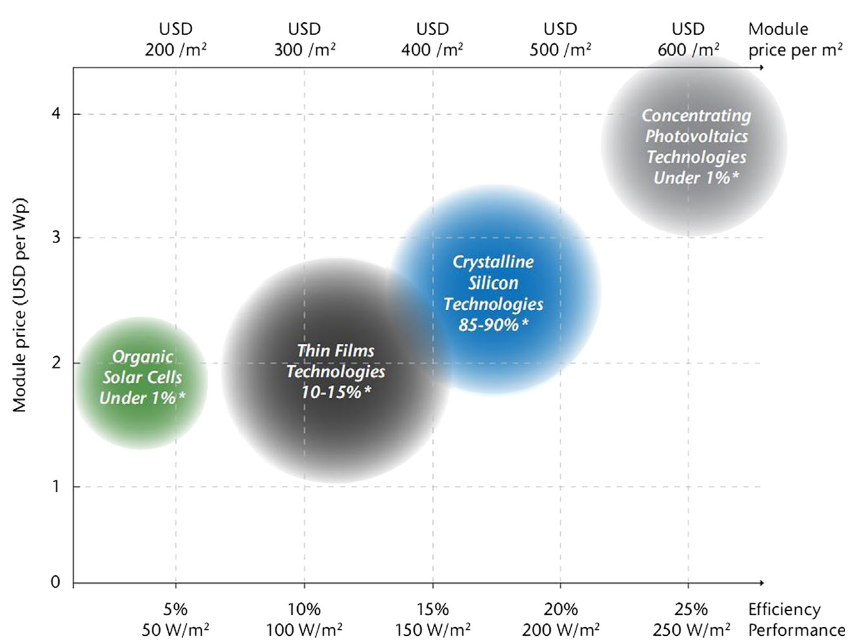


Fig. 1. Current performance and price of different PV module technologies [33].

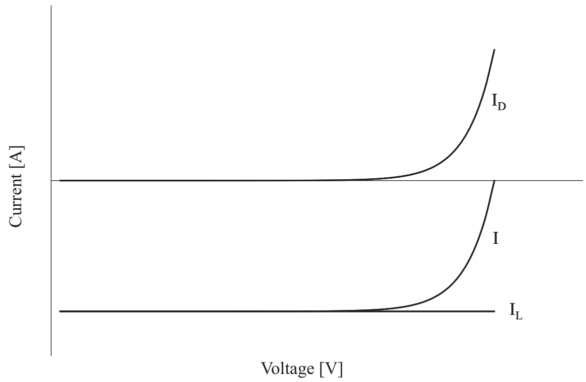


Fig. 2. *I–V* Characteristic of a diode and illuminated cell.

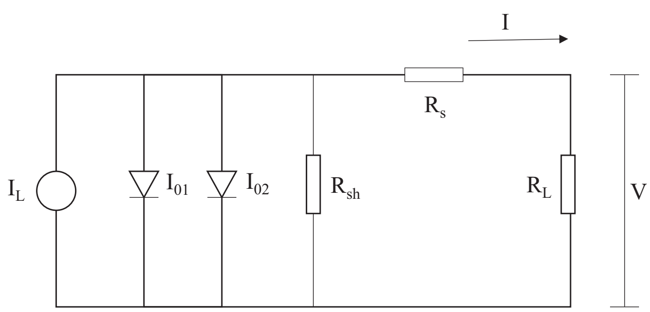


Fig. 3. Schema of simplified two diodes equivalent circuit.

implicit form of the equation and by the presence of two exponential terms. In the scientific literature, there are few fully explained models that permit coding of the algorithm to retrieve the seven parameters; furthermore, these models concern the single cell and are based on particular assumptions that limit their application. Indeed, some authors admit that the initial conditions strongly affect the resolution of Eq. (3) [38–40]. In these models, the procedures need to be properly guided during the initial estimation of the parameters to avoid inconsistent results.

For these reasons, some authors have preferred to employ different correlations not based on an electric model [41–42], whereas others have used a simplified model based on a single diode [15–19], as shown in Fig. 4. This new equivalent circuit is described by the following implicit equation:

$$I = I_L - I_0\left(e^{\frac{V+IR_s}{nT}} - 1\right) - \frac{V+IR_s}{R_{sh}} \tag{4}$$

in which there are only five unknown parameters and only one exponential term. According to the traditional approach, the photocurrent I_L depends on the irradiance, I_0 is affected by the temperature of the cell and n, R_s and R_{sh} are constant.

Some authors have focused on studying the one-diode model and have suggested some directions for improvement and/or simplification that would allow determination of the five parameters (I_L, n, I_0, R_s, R_{sh}) based on the performance data of the modules commonly provided by the manufacturers. Here, we review five of the best explained models available in the literature for the evaluation of the electrical behaviour of a single junction-based PV module. The models proposed by De Blas et al. [15] (par. 3.1), Hadj Arab et al. [16] (par. 3.2), De Soto et al. [17] (par. 3.3), Villalva et al. [18] (par. 3.4) and Lo Brano et al. [19] (par. 3.5) will be described in detail.

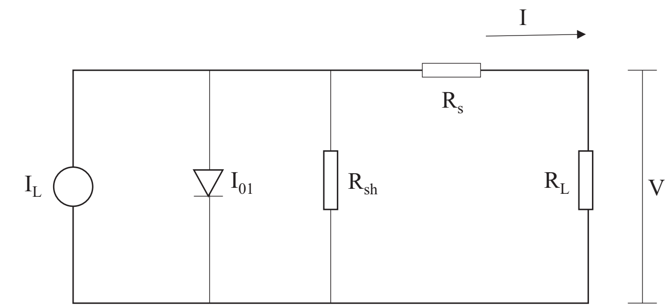


Fig. 4. Schema of one-diode simplified equivalent circuit.

3.1. De Blas, Torres, Pieto and Garcìa model

In [15], De Blas et al. address the study of the electrical behaviour of a PV panel determining the five parameters solving an equations system and applying some modifications and simplifications to the traditional model. De Blas et al. state that their model permits to obtain a series of *I–V* curves taking into account the environmental variability with errors less than 1% in comparison with experimental results.

Three of the five equations of the system, are determined imposing that the following points belong to the *I–V* curve, expressed by Eq. (4):

1. Open circuit point: ($V = V_{OC}$, $I = 0$);
2. Short circuit point ($V = 0$, $I = I_{SC}$);
3. Maximum power point($V = V_{mp}$, $I = I_{mp}$).

In these cases, Eq. (4) becomes

$$0 = I_L - I_0\left(e^{\frac{V_{OC}}{nT}} - 1\right) - \frac{V_{OC}}{R_{sh}} \tag{5}$$

$$I_{SC} = I_L - I_0\left(e^{\frac{I_{SC}R_s}{nT}} - 1\right) - \frac{I_{SC}R_s}{R_{sh}} \tag{6}$$

$$I_{mp} = I_L - I_0\left(e^{\frac{V_{mp}+I_{mp}R_s}{nT}} - 1\right) - \frac{V_{mp}+I_{mp}R_s}{R_{sh}} \tag{7}$$

The substitution in Eq. (6) of the value of the photocurrent derived from Eq. (5) yields the following:

$$I_{SC}\left(1+\frac{R_s}{R_{sh}}\right) = I_L - I_0\left(e^{\frac{I_{SC}R_s}{nT}} - 1\right) = I_0\left(e^{\frac{V_{OC}}{nT}} - 1\right) + \frac{V_{OC}}{R_{sh}} - I_0\left(e^{\frac{I_{SC}R_s}{nT}} - 1\right)$$

$$I_{SC}\left(1+\frac{R_s}{R_{sh}}\right) - \frac{V_{OC}}{R_{sh}} = I_0\left(e^{\frac{V_{OC}}{nT}} - 1 - e^{\frac{I_{SC}R_s}{nT}} + 1\right)$$

Then,

$$I_0 = \left[I_{SC}\left(1+\frac{R_s}{R_{sh}}\right) - \frac{V_{OC}}{R_{sh}}\right] \Big/ \left(e^{\frac{V_{OC}}{nT}} - e^{\frac{I_{SC}R_s}{nT}}\right)$$

assuming that

$$e^{\frac{V_{OC}}{nT}} \gg e^{\frac{I_{SC}R_s}{nT}} \tag{8}$$

De Blas et al. hypothesise that

$$I_0 = \left[I_{SC}\left(1+\frac{R_s}{R_{sh}}\right) - \frac{V_{OC}}{R_{sh}}\right] \Big/ e^{\frac{V_{OC}}{nT}} \tag{9}$$

Similarly, substituting Eq. (7) the same value of the photocurrent, the equation becomes

$$I_{mp} = I_0\left(e^{\frac{V_{OC}}{nT}} - 1\right) + \frac{V_{OC}}{R_{sh}} - I_0\left(e^{\frac{V_{mp}+I_{mp}R_s}{nT}} - 1\right) - \frac{V_{mp}+I_{mp}R_s}{R_{sh}} \tag{10}$$

Furthermore, substituting Eq. (9) in Eq. (10) yields the following:

$$I_{mp} = \left[I_{SC}\left(1+\frac{R_s}{R_{sh}}\right) - \frac{V_{OC}}{R_{sh}}\right]\left[1 - e^{\frac{V_{mp}+I_{mp}R_s-V_{OC}}{nT}}\right] + \frac{V_{OC}-V_{mp}}{R_{sh}} - \frac{I_{mp}R_s}{R_{sh}}$$

or else

$$I_{mp}\left(1+\frac{R_s}{R_{sh}}\right) - I_{SC}\left(1+\frac{R_s}{R_{sh}}\right) + \frac{V_{OC}}{R_{sh}} - \frac{V_{OC}-V_{mp}}{R_{sh}} = \left[I_{SC}\left(1+\frac{R_s}{R_{sh}}\right) - \frac{V_{OC}}{R_{sh}}\right]\left[1 - e^{\frac{V_{mp}+I_{mp}R_s-V_{OC}}{nT}}\right]$$

After some mathematical manipulation, it is possible to state the following:

$$nT = \frac{V_{mp}+I_{mp}R_s-V_{OC}}{\ln\left(\frac{(I_{mp}-I_{SC})(1+R_s/R_{sh})-(V_{mp}/R_{sh})}{I_{SC}(1+R_s/R_{sh})-(V_{OC}/R_{sh})}\right)} \tag{11}$$

The other two conditions that permit solving the equation system are determined by imposing the equality of the derivative of Eq. (4) at short circuit and open circuit points, respectively, with the reciprocal of the slopes of the characteristic curve in these points; these values are called R_{sh0} and R_{s0}, and they can be graphically evaluated from the experimental I–V curves issued by the manufacturers.

4. The derivative at the short circuit point is as follows:

$$\left.\frac{dI}{dV}\right|_{V=0} = -\frac{\frac{I_0}{nT}\exp^{\frac{I_{SC}R_s}{nT}} + \frac{1}{R_{sh}}}{1+R_s\left(\frac{I_0}{nT}\exp^{\frac{I_{SC}R_s}{nT}} + \frac{1}{R_{sh}}\right)} = -\frac{1}{R_{sh0}} \tag{12}$$

5. The derivative at the open circuit point is as follows:

$$\left.\frac{dI}{dV}\right|_{V=V_{OC}} = -\frac{\frac{I_0}{nT}e^{\frac{V_{OC}}{nT}} + \frac{1}{R_{sh}}}{1+R_s\left(\frac{I_0}{nT}e^{\frac{V_{OC}}{nT}} + \frac{1}{R_{sh}}\right)} = -\frac{1}{R_{s_0}} \tag{13}$$

3.1.1. Mathematical and physical assumptions

Furthermore, to simplify the equation system, De Blas hypothesises that

$$\frac{I_0}{nT}e^{\frac{I_{SC}R_s}{nT}} \ll \frac{1}{R_{sh}} \tag{14}$$

so Eq. (12) becomes

$$\left.\frac{dI}{dV}\right|_{V=0} = \frac{1/R_{sh}}{1+(R_s/R_{sh})} = \frac{1}{R_{sh0}},$$

Finally, it is possible to state that

$$R_{sh} = R_{sh0} - R_s \tag{15}$$

Substituting Eq. (9) into Eq. (13) yields the following:

$$\frac{1}{R_{s_0}} = \frac{\frac{\frac{I_{SC}(R_{sh}+R_s)-V_{OC}}{R_{sh}nT}}{nT} + \frac{1}{R_{sh}}}{R_{sh}+R_s\frac{\frac{I_{SC}\left(\frac{(R_{sh}+R_s)}{R_{sh}}\right)-V_{OC}}{nT}+1}{R_{sh}}}$$

and because the value of Eq. (15) can be expressed as function of the resistances R_{sh0} and R_{s0}, the last equation can be rewritten as follows:

$$\frac{1}{R_{s_0}} = \frac{\frac{I_{SC}(R_{sh0}-R_s+R_s)-V_{OC}}{nT}+1}{R_{sh0}-R_s+R_s\left[\frac{I_{SC}(R_{sh0}-R_s+R_s)-V_{OC}}{nT}+1\right]}$$

$$R_s\frac{I_{SC}R_{sh0}-V_{OC}}{nT} + R_{sh0} = R_{s_0}\left[1+\frac{I_{SC}R_{sh0}-V_{OC}}{nT}\right].$$

Explicating R_s results in the following:

$$R_s = \frac{R_{s_0}\left[\frac{V_{OC}}{nT}-1\right] + R_{sh0}\left[1+\frac{I_{SC}R_{s_0}}{nT}\right]}{\frac{V_{OC}-I_{SC}R_{sh0}}{nT}} \tag{16}$$

The previous simplifications that have been adopted to determine the unknown parameters, $e^{\frac{V_{OC}}{nT}} \gg e^{\frac{I_{SC}R_s}{nT}}$ and $\frac{I_0}{nT}e^{\frac{I_{SC}R_s}{nT}} \ll \frac{1}{R_{sh}}$ are usually fully satisfied.

3.1.2. The algorithm steps

With this approach, adopting an iterative process that provides the initial estimate of R_s value, the De Blas et al. model retrieves the five unknown parameters. In detail, the algorithm steps are as follows:

- a starting R_s value is hypothesised;
- n and R_{sh} values are calculated from Eqs. (11) and (15);
- R_s value is recalculated with Eq. (16);
- an iterative procedure verifies the convergence of R_s value;
- when R_s converges, the correct value of R_{sh} is recalculated; and
- the values of I_L and I_0.are calculated using Eqs. (5) and (9).

To describe the behaviour of a PV module at different conditions of temperature and radiation, De Blas et al. suggest the application of the procedure described by the International Standards IEC891 [43] that, starting from the knowledge of current and voltage values for the given temperature and irradiance, defines the variation of the I–V characteristics. To adapt the saturation current of the diode I_0 with a variable temperature conditions, IEC891 uses the Townsend equation [44]:

$$I_0(T) = D\,T^3 e^{\left(\frac{q\varepsilon_{ref}}{AkT}\right)} \tag{17}$$

in which ε_{ref} is the material band-gap energy (1.12 eV for silicon) at Standard Reference Conditions (SRC), $A=\gamma N_s$ where γ is the completion or shape factor and N_s is the number of cells wired in series (for ideal cell A is equal 1) and D is the diode diffusion factor (approximately constant). Therefore, on the basis of the correct evaluation ofI_0, R_s and R_{sh}, the other parameters can be derived using the values of V_{oc} and I_{sc} at new conditions (Eqs. (5) and (6)).

With these assumptions, the parameters that are variable with temperature and/or irradiance are I_0, I_{SC} and n. This last parameter, which should be considered independent of temperature, can be evaluated only if the values of I_{mp} and V_{mp} are known in non-standard conditions.

3.2. Hadj Arab, Chenlo and Benghanem model

In [16], Hadj Arab et al. proposed a five parameter model that is detailed described and experimented in [45]. In this last work the electrical behaviour of a PV panel by referring to an equivalent electric circuit which includes the photocurrent, the reverse saturation current and the series and in parallel resistances. Indeed the experimental test show how the traditional model with five parameters leads to more accurate assessments of operating current and more faithfully describes the behaviour of a photovoltaic panel especially during the maximum irradiance

In this case, Eq. (4) has been rewritten in a different form:

$$I = I_L - I_0\left(e^{\frac{V+IR_s}{mV_t}} - 1\right) - \frac{V+IR_s}{R_{sh}} \tag{18}$$

in which the five unknown parameters of the model proposed in [25] are I_L, I_0, R_s, R_{sh} and m when

$$m = \frac{[V_{mp}+I_{mp}R_{s0}-V_{OC}]}{V_t\left[\ln\left(I_{SC}-\frac{V_{mp}}{R_{sh}}-I_{mp}\right) - \ln\left(I_{SC}-\frac{V_{OC}}{R_{sh}}\right) + \frac{I_{mp}}{I_{SC}-(V_{OC}/R_{sh0})}\right]} \tag{19}$$

To determine the values of these parameters, the three known I–V pairs at SRC are imposed in Eq. (18): open circuit point ($V=V_{OC}$, $I=0$); short circuit point ($V=0$, $I=I_{SC}$) and maximum power point ($V=V_{mp}$, $I=I_{mp}$). Furthermore the resistance definitions used in Eqs. (12) and (13) are applied; where R_{s0} and R_{sh0} are the inverse of the slope in the open circuit point and in the short-circuit point, respectively; these assumptions lead to a different form of Eqs. (12) and (13) in which nT is substituted by mV_t.

3.2.1. Mathematical and physical assumptions

To simplify the solution of this system in the model the following considerations are applied:

If

$$\frac{1}{R_{sh}} \ll \frac{I_0}{mV_t} e^{\frac{V_{OC}}{mV_t}} \tag{20}$$

Eq. (13) becomes

$$\frac{\frac{I_0}{mV_t} e^{\frac{V_{OC}}{mV_t}}}{1+R_s \frac{I_0}{mV_t} e^{\frac{V_{OC}}{mV_t}}} = \frac{1}{R_{s0}}; \quad R_{s0}\frac{I_0}{mV_t} e^{\frac{V_{OC}}{mV_t}} = 1 + R_s \frac{I_0}{mV_t} e^{\frac{V_{OC}}{mV_t}}; \quad R_s = R_{s0} - \frac{1}{\frac{I_0}{mV_t} e^{\frac{V_{OC}}{mV_t}}}.$$

So

$$R_s = R_{s0} - \frac{mV_t}{I_0} e^{-\frac{V_{OC}}{mV_t}} \tag{21}$$

Similarly, if

$$\frac{I_0}{mV_t} e^{\frac{I_{SC}}{mV_t}} \cong 0 \tag{22}$$

Eq. (12) can be rewritten as follows:

$$\frac{1/R_{sh}}{1+(R_s/R_{sh})} = \frac{1}{R_{sh0}}; \quad \frac{1}{R_s+R_{sh}} = \frac{1}{R_{sh0}}$$

So,

$$R_{sh} = R_{sh0} - R_s \tag{23}$$

Furthermore if

$$R_s \ll R_{sh} \rightarrow R_{sh0} \cong R_{sh} \tag{24}$$

Similarly, if

$$e^{\frac{V_{OC}}{mV_t}} \gg 1 \tag{25}$$

in Eq. (5), and $I_L \cong I_{SC}$, then

$$I_0 = \frac{I_L - \frac{V_{OC}}{R_{sh}}}{e^{\frac{V_{OC}}{mV_t}}} = \left(I_{SC} - \frac{V_{OC}}{R_{sh}}\right) e^{-\frac{V_{OC}}{mV_t}} \tag{26}$$

Knowing I_0, Eq. (7) can be rewritten as follows:

$$I_{mp} = I_{SC} - \frac{I_{SC} - \frac{V_{OC}}{R_{sh}}}{e^{\frac{V_{OC}}{mV_t}}}\left(e^{\frac{V_{mp}+I_{mp}R_s}{mV_t}} - 1\right) - \frac{V_{mp}+I_{mp}R_s}{R_{sh}}$$
$$= I_{SC} - \left(I_{SC} - \frac{V_{OC}}{R_{sh}}\right)\left(e^{\frac{V_{mp}+I_{mp}R_s-V_{OC}}{mV_t}} - e^{-\frac{V_{OC}}{mV_t}}\right) - \frac{V_{mp}+I_{mp}R_s}{R_{sh}}$$

If

$$e^{\frac{V_{mp}+I_{mp}R_s}{mV_t}} \gg 1 \tag{27}$$

then the term $e^{-\frac{V_{OC}}{mV_t}}$ can be neglected:

$$\left(I_{SC} - \frac{V_{OC}}{R_{sh}}\right) e^{\frac{V_{mp}+I_{mp}R_s-V_{OC}}{mV_t}} = I_{SC} - \frac{V_{mp}}{R_{sh}} - I_{mp}\left(1 - \frac{R_s}{R_{sh}}\right)$$

Finally, if

$$\frac{R_s}{R_{sh}} \ll 1 \tag{28}$$

using the definition of R_s in Eq. (21),

$$\left(I_{SC} - \frac{V_{OC}}{R_{sh}}\right) e^{\frac{V_{mp}+I_{mp}R_{s0} - \frac{I_{mp}mV_t}{I_{SC}-\frac{V_{OC}}{R_{sh}}} - V_{OC}}{mV_t}} = I_{SC} - \frac{V_{mp}}{R_{sh}} - I_{mp};$$
$$e^{\frac{V_{mp}+I_{mp}R_{s0}-V_{OC}}{mV_t}} e^{-\frac{I_{mp}}{I_{SC}-\frac{V_{OC}}{R_{sh}}}} = \frac{\left(I_{SC} - \frac{V_{mp}}{R_{sh}} - I_{mp}\right)}{\left(I_{SC} - \frac{V_{OC}}{R_{sh}}\right)}$$

or rather

$$\frac{V_{mp}+I_{mp}R_s-V_{OC}}{mV_t} - \frac{-I_{mp}mV_t}{mV_t\left(I_{SC}-\frac{V_{OC}}{R_{sh}}\right)} = \ln\left[\frac{I_{SC}-\frac{V_{mp}}{R_{sh}}-I_{mp}}{I_{SC}-\frac{V_{OC}}{R_{sh}}}\right] \tag{29}$$

Thus, it is possible to obtain the definition of mV_t as explained in Eq. (19).

To solve the system formed by Eqs. (6), (19), (24), (29) and (26), is necessary to know the values of I_{SC} and V_{OC}. These parameters are considered variables with irradiance and temperature:

$$I_{sc} = I_{sc,SRC}\frac{G}{G_{SRC}} + \mu_{I_{SC}}(T - T_{SRC}) \tag{30}$$

$$V_{OC} = V_{OC,SRC} + mV_t \ln\left(\frac{G}{G_{SRC}}\right) + \mu_{V_{OC}}(T - T_{SRC}) \tag{31}$$

3.2.2. The algorithm steps

The calculation procedure can be summarised as follows:

- the R_{sh} value is calculated by Eq. (24);
- I_{SC} and V_{OC} parameters are calculated by Eqs. (30) and (31);
- mV_t is obtained knowing R_{s0} , I_{SC}, V_{OC}, current and voltage at the maximum power point and using Eq. (19);
- R_s is obtained with Eq. (21); and
- I_0 is obtained from Eq. (26);
- Finally, I_L is obtained from Eq. (6).

3.3. De Soto, Klein and Beckman model

De Soto et al. propose a model in [17] for the evaluation of the performance of a PV panel represented by a one-diode equivalent circuit in which the current–voltage relationship for fixed cell temperature and irradiance is expressed by the following equation:

$$I = I_L - I_0\left(e^{\frac{V+IR_s}{a}} - 1\right) - \frac{V+IR_s}{R_{sh}} \tag{32}$$

where a is an ideality factor defined as follows:

$$a = \frac{N_s nkT}{q} \tag{33}$$

Even in this model, the solution of the five parameter problem implies the application of some conditions that refer to the points of open circuit ($V=V_{OC}$, $I=0$), short circuit ($V=0$, $I=I_{SC}$)and the current and voltage at the maximum power point ($V=V_{mp}$, $I=I_{mp}$) evaluated at SRC. The first three equations of the system are as follows:

$$I_L - I_0\left(e^{\frac{V_{OC}}{a}} - 1\right) - \frac{V_{OC}}{R_{sh}} = 0 \tag{34}$$

$$I_{SC} = I_L - I_0\left(e^{\frac{V_{OC}\,R_s}{a}} - 1\right) - \frac{V_{OC}R_s}{R_{sh}} \tag{35}$$

$$I_{mp} = I_L - I_0\left(e^{\frac{V_{mp}+I_{mp}\,R_s}{a}} - 1\right) - \frac{V_{mp}+I_{mp}\,R_s}{R_{sh}} \tag{36}$$

where a represents the ideality factor and I_L is the value of the photocurrent under SRC.

Because these relations are insufficient for the determination of the five parameters (I_L, n, I_0, R_s, R_{sh}), further equations are obtained by imposing the derivative of the power curve at the maximum point equal to zero and giving as known the coefficient value of the thermal variation of V_{OC}:

$$\left.\frac{dP}{dV}\right|_{P=P_{max}} = I_{mp} + V_{mp}\left.\frac{dI}{dV}\right|_{mp} = 0 \tag{37}$$

The last conditions use the expression of the thermal drift of the open-circuit voltage:

$$\mu_{V_{oc}} = \left.\frac{dV}{dT}\right|_{I=0} \approx \frac{V_{OC,\,SRC} - V_{OC,T}}{T_{SRC} - T} \tag{38}$$

where T_{SRC} is the temperature at SRC.

To determine $\mu_{V_{oc}}$, it is necessary to know the value of the open circuit voltage $V_{OC,T}$. Because the parallel resistance R_{sh} was assumed to be independent of temperature, to determine the value of $V_{OC,T}$ using Eq. (32) and then to solve Eq. (37), it is necessary to know the dependency of the parameters a, I_0 and I_L, with temperature.

3.3.1. Mathematical and physical assumptions

To this aim, the De Soto model takes into account the following assumptions:

a) The value of ideality factor a is deduced from the temperature of the cell T. In particular, for any operating condition, it is a linear function of the temperature of the cell:

$$\frac{a}{a_{SRC}} = \frac{T}{T_{SRC}} \tag{39}$$

b) The variation of the current with the operating temperature is explained by the following equation:

$$\frac{I_0}{I_{0,SRC}} = \left[\frac{T}{T_{SRC}}\right]^3 e^{\frac{1}{k}\left[\frac{\varepsilon_{SRC}}{T_{SRC}} - \frac{\varepsilon}{T}\right]} \tag{40}$$

in which the ratio between the current at any conditions and the current obtained at reference conditions $I_{0,SRC}$ depends on the ratio between the temperatures and on an exponential term.

In detail, the reverse current saturation is evaluated with a relation that is derived from the Townsend equation Eq. (17). In Millman-Halkias [46], it is stated that

$$I_0 \cong K\, T^m e^{\frac{qV_{GO}}{\eta kT}} \tag{41}$$

where K is a constant and $qV_{GO} = \varepsilon_{SRC}$ is the amplitude in joule of energy gap; for silicon, the values of η and m are 2 and 1.5, respectively. Substituting the value of $V_T = kTN_s/q$ into Eq. (17) and Eq. (41), it is possible to state that $K = D$, $m = 3$, $\eta = n$. Furthermore, for an ideal cell, the equation becomes

$$I_{0,SRC} = D\, T_{SRC}^3 e^{\frac{q}{k}\frac{\varepsilon_{SRC}}{T_{SRC}}} \tag{42}$$

Substituting Eq. (42) into Eq. (40), it is possible to obtain the relationship that describes the dependence of the current I_0 on the operating temperature of the system:

$$\frac{I_0}{I_{0,SRC}} = \frac{DT^3 e^{\frac{q}{k}\frac{\varepsilon}{T}}}{DT^3 e^{\frac{q}{k}\frac{\varepsilon_{SRC}}{T_{SRC}}}} = \left[\frac{T}{T_{SRC}}\right]^3 e^{\frac{1}{k}\left[\frac{q}{}\frac{\varepsilon_{SRC}}{T_{SRC}} - \frac{q}{}\frac{\varepsilon}{T}\right]} \tag{43}$$

c) The determination of the photocurrent I_L is obtained as a function of short-circuit current thermal drift $\mu_{I_{sc}}$. In particular, the expression that allows the determination of this variable is as follows:

$$I_L = \frac{G}{G_{SRC}}\frac{M}{M_{SRC}}\left[I_{L,SRC} + \mu_{I_{SC}}(T - T_{SRC})\right] \tag{44}$$

where G represents the irradiance and M is the modified air mass (M is an index derived as function of air mass, zenith angle of the photovoltaic system and of four constants typical of each type of panel; these parameters were experimentally obtained from NIST – Fanney et al. [47]).

Finally, to complete the model, De Soto et al. have analysed the dependence of the resistances R_s and R_{sh} with the operating conditions. The R_s influences the shape of the I–V curves near the maximum power point. In [17], De Soto et al. show how, by varying R_s by 20% (in excess or in deficit) with respect to the reference value, the effect on the curve is practically insignificant, thus justifying the assumption that R_s can be treated as a constant. R_{sh} determines the slope of the I–V curve in the short circuit condition, becoming more horizontal as it increases. In [17], the authors claim that its value seems to vary with the irradiance G for all types of cells; in particular, De Soto et al. refer to the Schroder definition [48], which indicates that, for low values of irradiance, the value of R_{sh} is inversely proportional to the short-circuit current and therefore to the irradiance. For a description of this phenomenon, the De Soto et al. model proposes the following expression:

$$\frac{R_{sh}}{R_{sh,SRC}} = \frac{G_{SRC}}{G} \tag{45}$$

3.3.2. The algorithm steps

Knowing the dependence of a, I_0 and I_L on temperature (Eqs. (39), (40) and (44)), and of R_s and R_{sh} on the operating conditions, the solution of the system of five equations (Eqs. (34)–(37) and (38)) with five unknowns is solved by a nonlinear solver, the Engineering Equation Solver – EES [49].

However, the operating procedure adopted to solve this equations system represents a weak point in the model.

3.4. Villalva, Gazoli and Filho model

In [18], Villalva et al. propose a model to determine the parameters of the nonlinear I–V, shown in Eq. (32), by adjusting the curve at three remarkable points: open circuit, maximum power and short circuit points provided by the manufacturer. Given these three points, which are provided in all commercial array datasheets, the method aims to find the best I–V equation including the effect of the series and parallel resistances, and warranties that the maximum power of the model matches the maximum power of the real array.

3.4.1. Mathematical and physical assumptions

Two other conditions are necessary to solve the system of equations. In [18,50], the authors propose the following assumptions:

- The I_L current of the PV cell depends linearly on the irradiance and the temperature according to the following equation:

$$I_L = [I_{L,\,SRC} + \mu_{I_{SC}}(T - T_{SRC})]\frac{G}{G_{SRC}} \tag{46}$$

- The authors propose a new expression of I_0 :

$$I_0 = \frac{I_{SC,SRC} + \mu_{I_{SC}}(T - T_{SRC})}{e^{\frac{V_{OC,SRC} + \mu_{V_{OC}}(T - T_{SRC})}{aV_t}} - 1} \tag{47}$$

Usually, $1 \le a \le 1.5$ because a expresses the degree of ideality of the diode, and it is totally empirical; any initial value can be chosen to adjust the model. Eq. (47) proposes a different approach to express the dependence of I_0 on temperature and the thermal drift of voltage.

3.4.2. The algorithm steps

In [18,50], the authors propose an algorithm for adjusting the resistance values based on the fact that there is only one pair $\{R_s, R_{sh}\}$ that assures that the calculated maximum power is equal to the maximum experimental power. The authors claim that the proposed model is further improved by taking advantage of the following iterative solution of R_s and R_{sh}: R_s is slowly incremented starting from $R_s \cong 0$; the initial value of R_{sh} is given by the following:

$$R_{sh,\ min} = \frac{V_{mp}}{I_{SC,SRC} - I_{mp}} - \frac{V_{OC,SRC} - V_{mp}}{I_{mp}} \tag{48}$$

Each iteration updates R_s and R_{sh} towards the best model solution. The initial guess of $I_{L,SRC}$ is obtained by the following relationship:

$$I_{L,SRC} = \frac{R_s + R_{sh}}{R_{sh}} I_{SC,SRC} \tag{49}$$

The values of R_s and R_{sh} are initially unknown, but as the solution of the algorithm is refined along successive iterations, the values of R_s and R_{sh} tend towards the best solution, and Eq. (49) becomes valid and effectively determines the light-generated current I_L while taking into account the influence of the series and parallel resistances of the array. The software coding this algorithm is available in [51].

3.5. Lo Brano, Orioli, Ciulla and Di Gangi model

Lo Brano et al. propose, in [19], a model for the evaluation of the performance of a PV panel represented by a one-diode equivalent circuit in which it is postulated that R_s, R_{sh} and I_0 change with the irradiance; this hypothesis is realistic because a PV cell and an illuminated semiconductor diode have different electrical behaviours. Based on these assumptions, a new five parameter model is proposed, and it is described by the following equation:

$$I(\alpha_G, T) = \alpha_G I_L(T) - I_0(\alpha_G, T)\left(e^{\frac{\alpha_G[V + J\ I(T - T_{SRC})] + I\ R_s}{\alpha_G n T}} - 1\right) - \frac{\alpha_G[V + J\ I(T - T_{SRC})] + I\ R_s}{R_{sh}} \tag{50}$$

where $\alpha_G = G/G_{SRC}$ represents the ratio between the generic irradiance G and the irradiance at SRC G_{SRC}, and $I_L(T)$ is the photocurrent that can be evaluated by the following relation:

$$I_L(T) = I_{L,SRC} + \mu_{I_{SC}}(T - T_{SRC}) \tag{51}$$

3.5.1. Mathematical and physical assumptions

Although the authors suggest a linear relationship between the values of the series and shunt resistances and the irradiance, the following positions are made:

$$\begin{cases} R_s(\alpha_G) = \frac{R_{s,SRC}}{\alpha_G} \\ R_{sh}(\alpha_G) = \frac{R_{sh,SRC}}{\alpha_G} \end{cases} \tag{52}$$

Another important innovation concerns the determination of the value of $I_0(\alpha_G)$, which can be represented by the following equation:

$$I_0(\alpha_G, T) = \alpha_G \left(\frac{I_L(T) - \frac{V_{OC}(\alpha_G, T)}{R_{sh}}}{e^{\frac{V_{OC}(\alpha_G, T)}{nT}} - 1} \right) \tag{53}$$

The variability of V_{OC} with the temperature can be evaluated with the following equation:

$$V_{OC}(\alpha_G, T) = V_{OC,SRC}(\alpha_G, T) + \mu_{V_{OC}}(T - T_{SRC}) \tag{54}$$

Lo Brano et al. observed, in [19], that for numerous commercial panels, there is a regular dependence of the reverse saturation current with the irradiance and temperature expressed by the following formula:

$$I_0(\alpha_G; T) = \exp\left[\left(\frac{\alpha_G - 200}{1 - 0.2}\right) \ln \frac{I_0(1; T)}{I_0(0.2; T)} + \ln I_0(0.2; T)\right] \tag{55}$$

To better reproduce the I–V characteristic at generic temperature T, a thermal correction factor J is defined as follows:

$$J(\alpha_G, T) = \frac{V_{mp,SRC} - V_{mp}(\alpha_G, T)}{I_{mp}(T - T_{SRC})} \tag{56}$$

Here J is a thermal correction factor similar to the fill factor of the curve described by the IEC891 [43]. To determine the value of J, the value of T should be chosen based on the maximum or the minimum working temperature of the PV module and the maximum range of temperature within which the data from the manufacturer are provided (in [19], a temperature of 75 °C is considered).

3.5.2. The algorithm steps

The procedure to determine the five parameters requires a preliminary assessment of R_s and R_{sh}. It is also necessary to known the values of $I_{SC,SRC}$, $V_{OC,SRC}$, $I_{mp,SRC}$, $V_{mp,SRC}$ and the value of V_{OC} at standard temperature and at the lowest irradiance (typically 200 W/m^2); all these values can be graphically extracted from the standard I–V characteristic curve provided by the manufacturer. To determine J it is necessary to have the values of I_{mp} and V_{mp} at different temperatures with respect to SRC. To determine the values of the unknown parameters, the three known I–V pairs at SRC are imposed on Eq. (50), obtaining the same functional relationships as the Blas et al. model (Eqs. (5)–(7), (12) and (13)).

The system is solved numerically via a double cycle of iterations (trial and error) to retrieve the values of R_s and n. To initiate the solving procedure, the following positions are made:

$$\begin{cases} I_{L,SRC} = I_{SC,SRC} \\ R_{sh} = R_{sh0} \end{cases} \tag{57}$$

which is obtained by simplifying Eqs. (13) and (5) and taking into account the following:

$$\begin{cases} R_s \lll R_{sh0} \\ \frac{I_{0,SRC}\, e^{\frac{I_{0,SRC} R_s}{n T_{SRC}}}}{n T_{SRC}} \lll \frac{1}{R_{sh0}} \end{cases} \tag{58}$$

The procedure comprises the following steps:

1. first attempt values of n and of R_s are set;
2. $I_{L,SRC}$ and R_{sh} are calculated with Eq. (57);
3. $I_{0,SRC}$, $I_{L,SRC}$ and R_{sh} are derived in sequence, respectively from Eqs. (7), (6), and (12);
4. n is derived from Eq. (5), compared with the previous attempt value and is changed accordingly;
5. the trial and error process in steps 3 and 4 is reiterated until convergence of n is achieved with the desired accuracy;
6. once the first trial and error process for n has been completed, R_s is derived from Eq. (12), compared with the previous attempt value and changed accordingly;

Table 2
Synopsis of mathematical relationship employed for each model.

Five parameter models	***I–V* relationship for 1st, 2nd and 3rd conditions**		**4th condition**	**5th condition**
De Blas et al. **Hadj Arab et al.**	$\begin{cases} I = I(I_{SC}, 0) = 0 \\ I = I(0, V_{OC}) = 0 \\ I = I(I_{mp}, V_{mp}) = 0 \end{cases}$	$I = I_L - I_0\left(e^{\frac{V+IR_s}{nT}} - 1\right) - \frac{V+IR_s}{R_{sh}}$	$\frac{dI}{dV}\Big\|_{V=0} = -\frac{\frac{I_0}{nT}\exp^{\frac{I_{SC}R_S}{nT}} + \frac{1}{R_{sh}}}{1 + R_s\left(\frac{I_0}{nT}\exp^{\frac{I_{SC}R_S}{nT}} + \frac{1}{R_{sh}}\right)} = -\frac{1}{R_{sh0}}$	$\frac{dI}{dV}\Big\|_{V=V_{OC}} = -\frac{\frac{I_0}{nT}e^{\frac{V_{OC}}{nT}} + \frac{1}{R_{sh}}}{1 + R_s\left(\frac{I_0}{nT}e^{\frac{V_{OC}}{nT}} + \frac{1}{R_{sh}}\right)} = -\frac{1}{R_{s_0}}$
Lo Brano et al.		$I = \alpha_G I_L - I_0\left(e^{\frac{\alpha_G[V+JI(T-T_{SRC})]+IR_s}{\alpha_G nT}} - 1\right) - \frac{\alpha_G[V+JI(T-T_{SRC})]+IR_s}{R_{sh}}$		
De Soto et al. **Villalva et al.**		$I = I_L - I_0\left(e^{\frac{V+IR_s}{a}} - 1\right) - \frac{V+IR_s}{R_{sh}}$	$\frac{dP}{dV}\Big\|_{P=P_{max}} = 0$ $I_L = [I_{L,SRC} + \mu_{I_{SC}}(T - T_{SRC})]\frac{G}{G_{SRC}}$	$\mu_{V_{OC}} = \frac{dV}{dT}\Big\|_{I=0} \approx \frac{V_{OC,SRC} - V_{OC,T}}{T_{SRC} - T}$ $I_0 \frac{I_{sc,SRC} + \mu_{I_{SC}}(T - T_{SRC})}{e^{(V_{oc,SRC} + \mu_{V_{OC}}(T - T_{SRC})/aV_t)} - 1}$

7. the first trial and error process in steps 3–5 is again started and completely developed;
8. R_s is again derived from Eq. (12) and compared with the value of the previous attempt and changed accordingly; and
9. the second trial and error process for R_s is reiterated until the desired accuracy is achieved.

The system is solved in a non-approximate form because no simplified equations were used. The above procedure is coded into a short software routine using simple languages. It does not need to be guided towards solutions starting from initial fitted values of the searched parameters. The procedure is more reliable because it normalises all parameters with respect to V_{OC} and I_{SC}. Furthermore, in [52], the Lo Brano et al. model was validated with an experimental setup.

4. Discussion

In this section, the models described above are compared, highlighting their peculiarities while discussing the availability of initial data and the reliability of the results.

4.1. Availability of necessary input data

Each model is characterised by a system of five equations with five unknowns (I_L, n, I_0, R_s and R_{sh}). All considered models require the following three known points of the *I–V* curve: open circuit point, short circuit point and maximum power point. These points are always available in the datasheets provided by the manufacturers, and therefore, the obtainment of these necessary values is immediate.

- The De Blas, Hadj Arab and Lo Brano models require the measurement of the slope of the *I–V* curve at selected points: open and short circuit. Normally, the technical datasheets provided by the manufacturer do not include these data, and a graphic valuation must be carried out. This procedure is only possible if the datasheets provide a graphical representation of the *I–V* curve; however, a graphical estimation is always approximate, which produces a measurement error that can affect the results:
- The De Soto model also needs a graphical estimation of the *I–V* slope at the maximum power point and also requires the value of V_{OC}, the thermal drift coefficient. Although this value is generally available, relationship (38) is a finite numerical approximation of a derivative.
- On the other hand, the Villalva model requires the thermal drift coefficients of the open circuit voltage and short circuit current. These values are generally available in the official datasheets of commercial *PV* modules. This model does not require any graphical estimation.

Table 3
Mathematical and physical assumptions for each model.

	Assumptions
De Blas et al.	Eqs. (8), (14), (17)
Hadj Arab et al.	Eqs. (20), (22), (24), (25), (27), (28), (30), (31)
Lo Brano et al.	Eqs. (52)–(58)
De Soto et al.	Eqs. (39), (43), (44)
Villalva et al.	Eqs. (46)–(49)

4.2. Synopsis of the major hypothesis and simplifications

To facilitate the identification of the mathematical relationships that permit coding of the models into a software package, Tables 2 and 3 collect, for each model, the five fundamental equations used and their simplifications. As summarised in the first column of Table 2, all the models employ three remarkable known *I–V* pairs at SRC. These values are substituted in the fundamental equation; the second column of Table 2 collects for each model the mathematical function that links current and voltage, $I = I(I, V)$. The last two columns gather the fourth and the fifth conditions, which permits solution of the equation system:

- The De Blas et al. and the Hadj Arab et al. models are characterised by the same system of equations; however, the different physical and mathematical assumptions listed in Table 3 lead to different results. The fourth and fifth conditions concern the graphical valuation of *I–V* slope at short circuit and open circuit points.
- The first three equations employed by the De Soto at al. and Villalva et al. models are identical; nevertheless, the models use the thermal drift coefficients in different ways. The De Soto et al. model also uses the slope of the *P–V* curve at the maximum power point.
- Finally, the Lo Brano et al. model proposes a reformulation of the general fundamental equation that directly takes into account the effect of temperature and irradiance. The last two conditions are identical to those used by the De Blas et al. and the Hadj Arab et al. models.

4.3. Numerical performance

To assess the accuracy of each model with respect to the data provided by the manufacturer, the *I–V* and *P–V* curves at variable temperature and irradiance obtained by each model are

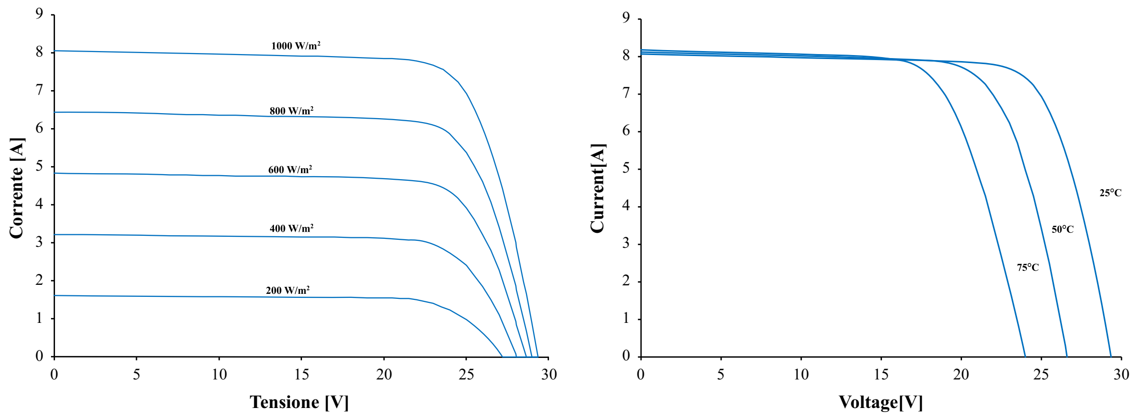


Fig. 5. *I–V* curves of the PV panel at constant temperature (25 °C) and at constant irradiance (1000 W/m^2).

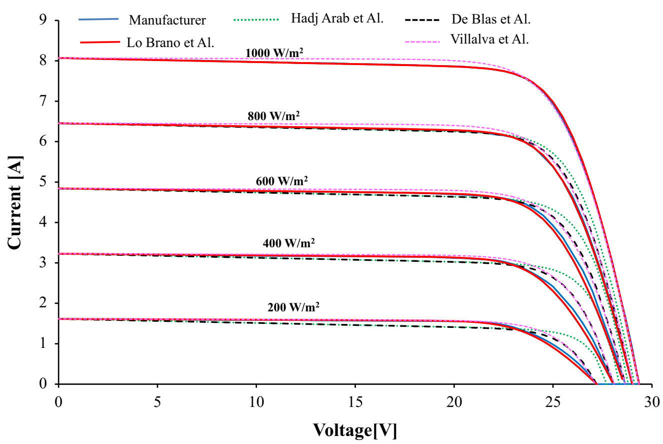


Fig. 6. *I–V* curves of a PV panel at variable irradiance and constant temperature.

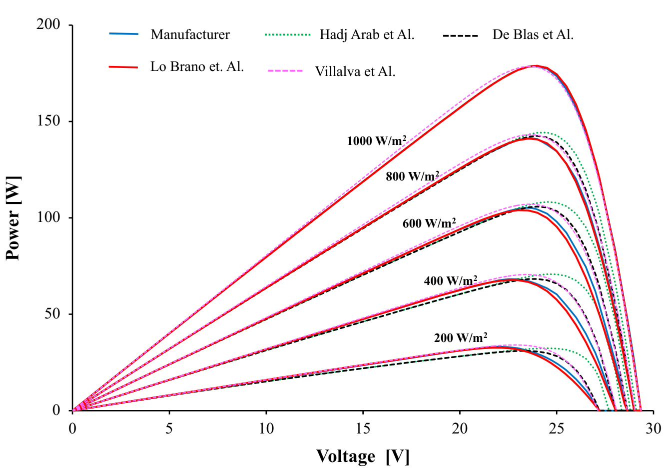


Fig. 7. *P–V* curves of a PV panel at variable irradiance and constant temperature.

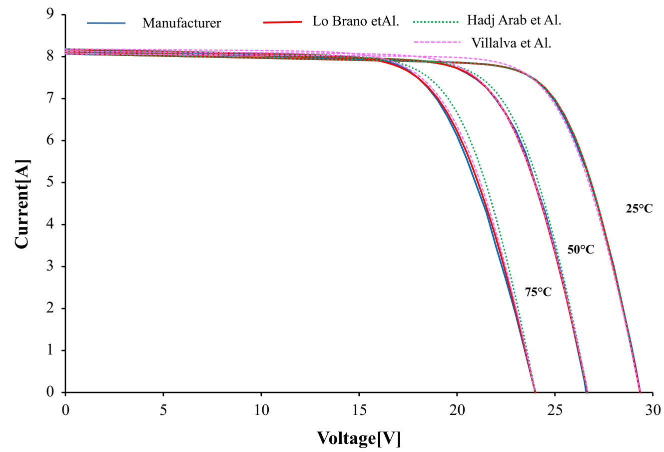


Fig. 8. *I–V* curves of PV panel at variable temperature and constant irradiance.

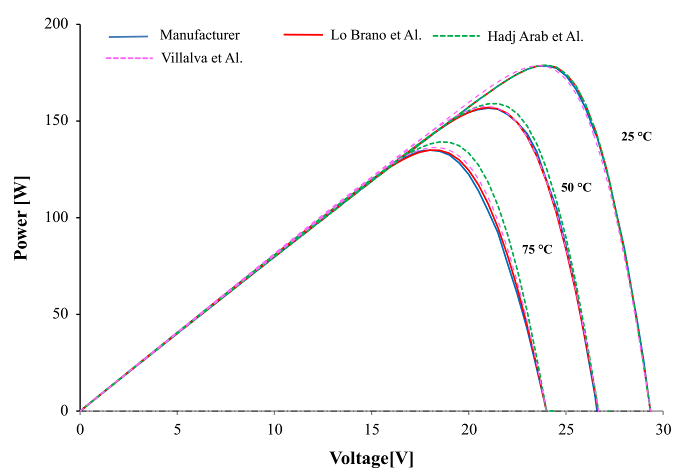


Fig. 9. *P–V* curves of a PV panel at variable temperature and constant irradiance.

represented in the following graphs (Figs. 6–9). In more detail, the authors used a specimen *PV* panel with the *I–V* curves drawn in Fig. 5 and the tabular data collected in Table 4.

Due to a lack of information regarding a detailed calculation procedure, it was impossible to obtain any numerical results from the De Soto et al. model.

The graphs above show that all of the models describe the *I–V* and *P–V* curves well when the irradiance is 1000 W/m^2 and the cell temperature is 25 °C. By varying the irradiance and/or the temperature, the agreement with the curves provided by the manufacturer changes considerably. Defining the mean absolute error as follows (Tables 5 and 6):

$$MAE = \frac{1}{N}\sum_{i=1}^{N}\left|\frac{P_{i,calculated} - P_{i,manufacturer}}{P_{i,manufacturer}}\right|$$

where *N* is the number of the samples, the following tables show the accuracy of each model with respect to the data issued by the manufacturer:

- Generally, the model that best describes the *I–V* and the *P–V* curves provided by the manufacturer is the Lo Brano et al. model, which is characterised by an MAE of 0.59 for the power

Table 4
Specimen PV panel characteristics.

	V_{OC} [V]	I_{SC} [A]	V_{max} [V]	I_{max} [A]	μ_{Voc} [V/°C]	μ_{Isc} [A/°C]
1000 W/m²	29.35	8.07	23.6	7.567	-1.07×10^{-1}	2.22×10^{-3}
200 W/m²	27.2	1.614	22	1.508		

Table 5
Mean absolute error at constant temperature (25 °C) between power data issued by the manufacturer and each model results.

	Mean average error					Global MAE
	200 W/m² K	400 W/m² K	600 W/m² K	800 W/m² K	1000 W/m² K	
De Blas	1.36	1.87	2.02	1.48	0.39	1.42
Hadj Arab	3.19	4.82	5.01	4.12	0.39	**3.51**
Lo Brano	0.41	0.68	1.06	0.40	0.39	**0.59**
Villalva	1.18	2.33	2.38	2.21	1.70	1.96

Table 6
Mean absolute error at constant irradiance (1000 W/m²) between power data issued by the manufacturer and each model results.

	Mean average error			Global MAE
	25 °C	50 °C	75 °C	
Hadj Arab	0.39	2.07	3.71	**2.05**
Lo Brano	0.39	0.53	0.82	**0.58**
Villalva	1.70	1.16	1.96	1.61

calculated at different values of irradiance and constant temperature and by an MAE of 0.58 for constant irradiance and different temperatures.

- The De Blas et al. and Hadj Arab et al. models tend to slightly underestimate the current and power values before the maximum power point; however, after the maximum power conditions, both models overestimate the currents and shift the curve slightly to the right. The De Blas model does not allow for calculation of the curve at variable temperatures.
- At the same time, the Villalva et al. model tends to overestimate the current and power values under any conditions other than SRC.

4.4. Overview of the models, hypothesis and simplifications

All examined models employed an iterative procedure to solve a system of five equations. However, each model is characterised by specific assumptions and simplifications that inevitably affect the results:

- The De Blas et al. model postulates that the quality factor n, which should be constant, varies with temperature and irradiance; in general, the value of n is known only at SRC (Eq. (11)). In practice, for each condition of irradiance and temperature, the model needs to be recalculated, estimating again the values of R_{s0} and R_{sh0}. To avoid uncertainty in the application of corrective methods, in [15], De Blas et al. validated their model using I_{SC} and V_{OC} values known under specific conditions of temperature and irradiance.
- The Hadj Arab et al. model is tested in [16]. This latest work is the one that best describes the proposed model and that best matches the electrical behaviour of a solar panel. Nevertheless, the model is characterised by several simplifications regarding the exponential terms that could affect the results. Furthermore, the model requires that the shunt resistance be much greater than the series resistance. This condition is generally always verified in a high quality PV module.
- In De Soto et al., the five parameters are determined through a nonlinear solver, a calculation tool that may have difficulty in solving the equation system. Some tests performed with automatic solvers have not led to automatic convergence. In addition, in the original article [17], there is not enough information about the calculation steps.
- Lo Brano et al. proposed a new five parameter model that was improved and corrected. The model is characterised by some significant differences, such as the variation of I_0, R_s and R_{sh} with irradiance and temperature. Application of the model allows for obtaining the best results in terms of comparison with the experimental *I–V* and *P–V* curves issued by manufactures.
- The aim of the Villalva at al. model is to fit the mathematical *I–V* equation to the experimentally remarkable point of the *I–V* curve of the practical array. A new empirical equation is proposed to calculate the reverse diode saturation current. Furthermore, an algorithm coded into a routine is available on the web for public download.

5. Concluding remarks

The *I–V* characteristics of a photovoltaic PV module can be reproduced assuming a one-diode equivalent circuit made of linear and non-linear components. In this paper, five of the most recent mathematical one-diode models for predicting the *I–V* curve of a PV cell, which take into account the variation of irradiance, electrical load and operating temperature, were examined in detail. These models reduce the problem to the determination of only five parameters: the photocurrent I_L, the diode saturation current I_0, the ideality factor n, and the series and parallel resistances R_s and R_{sh}.

The procedure for calculating these five electrical parameters constitutes the heart of the models examined, and this work allows for their evaluation with regard to the fundamental hypothesis, the availability of necessary data and the reliability of the results. For each model, the fundamental equations and the most important assumptions used were reported, and to simplify the analysis of the procedures, all equations were rewritten with the same nomenclature where possible. Finally, an accuracy analysis was performed to assess the capability of each model to reproduce the *I–V* curve of a specimen PV panel. This work permitted verification that all the models considered require numerical data that are not always available in the official datasheets. Some models require data obtainable only by applying semi-graphic procedures, thus leading to an inevitable uncertainty in the measured values. A common feature of all models evaluated in this paper is that, for solution of the system of five equations, they require the application of numerical techniques that may not converge if the first guess values are not sufficiently close to the real solution.

Concerning the reliability of the results, all of the models can reproduce the *I–V* curve at SRC with sufficient accuracy, although the Lo Brano et al. model is slightly more accurate than the others. However, although it is not particularly accurate in the calculation of the *I–V* and *P–V* curves, the Villalva et al. model does not require any graphic measurements, and a script is already available on the web.

References

[1] IEA: International Energy Agency. World energy outlook. 2012. ISBN 978-92-64-18084-0.
[2] Di Dio V, La Cascia D, Miceli R, Rando C. A mathematical model to determine the electrical energy production in photovoltaic fields under mismatch effect. In: Proceedings of IEEE-ICCEP 2007 international conference on clean electrical power. Capri, Italia; June 2009.
[3] Di Dio V, Miceli R, Rando C, Zizzo G. Dynamics photovoltaic generators: technical aspects and economical valuation. In: Proceedings of SPEEDAM 2010 International symposium on power electronics, electrical drives, automation and motion. Pisa, Italy; June 14–16, 2010.
[4] Lo Brano V, Orioli A, Ciulla G, Culotta S. Quality of wind speed fitting distributions for the urban area of Palermo, Italy. Renew Energy 2011;36(3).
[5] Griffith JS, Rathod NS, Paslaski J. Some tests on flat plate photovoltaic module cell temperatures in simulated field conditions. In: Proceedings of the 15th IEEE photovoltaic specialists conference. Kissimmee, FL;1981 May 12–15. p. 822.
[6] Lo Brano V, Ciulla G, Franzitta V, Viola A. A novel implicit correlation for the operative temperature of a PV panel. In: Proceedings of AASRI conference on power and energy systems, AASRI Procedia, vol. 2. September 2012.
[7] Skoplaki E, Palyvos JA. Operating temperature of photovoltaic modules: a survey of pertinent correlations. Renew Energy 2009;34(1):23–9.
[8] Eicker U. Solar technologies for buildings. 1st ed. Wiley; ISBN 0-471-48637-X.
[9] King DL. Sandia's PV module electrical performance model (version, 2000). Albuquerque, NM: Sandia National Laboratories; 2000.
[10] Database of Photovoltaic Module Performance Parameters. Sandia National Laboratories, 2002.
[11] Marion B, Anderberg M, George R, Gray-Hann P, Heimiller D. PVWATTS version 2 – enhanced spatial resolution for calculating grid-connected PV performance. NREL report NREL/CP-560-30941; 2001.
[12] Photovoltaic analysis and transient simulation method (PHANTASM). Solar Energy Laboratory, University of Wisconsin, Madison, WI; 1999.
[13] TRNSYS – Type 194. Five-parameter module. Solar Energy Laboratory, University of Wisconsin-Madison.
[14] PVsyst Photovoltaic software: 〈http://www.pvsyst.com/en/software〉.
[15] De Blas MA, Torres JL, Prieto E, Garcia A. Selecting a suitable model for characterizing photovoltaic devices. Renew Energy 2002;25:371–80.
[16] Hadj Arab A, Chenlo F, Benghanem M. Loss-of-load probability water pumping systems. Sol Energy 2004;76:713–72.
[17] De Soto W, Klein SA, Beckman WA. Improvement and validation of a model for photovoltaic array performance. Sol Energy 2006;80:78–88.
[18] Villalva MG, Gazoli JR, Filho ER. Comprehensive approach to modeling and simulation of photovoltaic arrays. IEEE Trans Power Electron 2009;24(5).
[19] Lo Brano V, Orioli A, Ciulla G, Di Gangi A. An improved five-parameter model for photovoltaic modules. Sol. Energy Mater. Sol. Cells 2010;94(8):1358–70.
[20] Easwarakhanthan T, Bottin J, Bouhouch I, Boutrit C. Non-linear minimization algorithm for determining the solar cell parameters with microcomputers. Int J Sol Energy 1986;4:1–12.
[21] Jacob Phang, Chan CH, Daniel SH. A review of curve fitting error criteria for solar cell *I–V* characteristics. Sol Cells 1986;18:1–12.
[22] Ikegami T, Maezono T, Nakanishi F, Yamagata Y, Ebihara K. Estimation of equivalent circuit parameters of PV module and its application to optimal operation of PV system. Sol Energy Mater Sol Cells 2001;67:389–95.
[23] Jervase Joseph A, Hadj Bourdoucen, Al-Lawati Ali. Solar cell parameter extraction using genetic algorithms. Meas Sci Technol 2001;12:1922–5.
[24] Zagrouba M, Sellami A, Bouaïcha M, Ksouri M. Identification of PV solar cells and modules parameters using the genetic algorithms: application to maximum power extraction. Sol Energy 2010;84(5):860–6.
[25] Ho WJ, Lin YJ, Chien LY, Lee YY, Chen YL, Yu CM, et al. 25.54% efficient single-junction GaAs solar cells using spin-on-film graded-index TiO_2/SiO_2 AR-coating. In: Proceedings of the quantum electronics and laser science conference. Optical Society of America; 2011.
[26] Bruton TM. General trends about photovoltaics based on crystalline silicon. Sol Energy Mater Sol Cells 2002;72(1):3–10.
[27] Parida B, Iniyan S, Goic R. A review of solar photovoltaic technologies. Renew Sustain Energy Rev 2011;15(3):1625–36.
[28] Dye-sensitized vs. thin film solar cell. European Instituted for Energy Research, 30 June 2006.
[29] Gregg BA, Hanna MC. Comparing organic to inorganic photovoltaic cells: theory, experiment, and simulation. J Appl Phys 2003;93(6):3605–14.
[30] Huynh WU, Dittmer JJ, Alivisatos AP. Hybrid nanorod-polymer solar cells. Science 2002;295(5564):2425–7.
[31] Semonin OE, Luther JM, Choi S, Chen HY, Gao J, Nozik AJ, et al. Peak external photocurrent quantum efficiency exceeding 100% via MEG in a quantum dot solar cell. Science 2011;334(6062):1530–3.
[32] Yeh N, Yeh P. Organic solar cells: their developments and potentials. Renew Sustain Energy Rev 2013;21:421–31.
[33] Technology Roadmap: Solar Photovoltaic Energy. OECD/IEA. 2010.
[34] NREL, Best research-cell efficiencies, 2013/3, downloaded 2013/03/18 from: 〈http://www.nrel.gov/ncpv/images/efficiency_chart.jpg〉.
[35] Shockley W. Electrons and holes in semiconductors. New York: Van Nostrand; 1950.
[36] Wolf M, Rauscenbach H. Series resistance effects on solar cell measurements. Adv Energy Convers 1963;3:455–79.
[37] McEvoy A, Markvart T, Castaner L. Practical handbook of photovoltaics: fundamentals and applications. Elsevier Science; 2011.
[38] Enebish N, Agchbayar D, Dorjkhand S, Baatar D, Ylemj I. Numerical analysis of solar cell current–voltage characteristics. Sol Energy Mater Sol Cells 1993;29:201–8.
[39] Hovinen A. Fitting of the solar cell IV-curve to the two diode model. Phys Scr 1994;T54:175–6.
[40] Garrido-Alzar CL. Algorithm for extraction of solar cell parameters from *I–V* curve using double exponential model. Renew Energy 1997;10(2/3):125–8.
[41] Akbaba M, Alattawi MAA. A new model for *I–V* characteristic of solar cell generators and its applications. Sol Energy Mater Sol Cells 1995;37:123–32.
[42] Ortiz-Conde O, Garcia Sanchez FJ, Muci J. New method to extract the model parameters of solar cells from the explicit analytic solutions of their illuminated *I–V* characteristics. Sol Energy Mater Sol Cells 2006;90:352–61.
[43] IEC 891 procedure for temperature and irradiance correction to measured *I–V* characteristic of silicon crystalline photovoltaic devices.
[44] Townsend TU. A method for estimating the long-term performance of direct-coupled photovoltaic systems [M.Sc. thesis]. Mechanical Engineering, University of Wisconsin-Madison; 1989.
[45] Naci Celik A, Acikgoz N. Modelling and experimental verification of the operating current of mono-crystalline photovoltaic modules using four- and five parameter models. Appl Energy 2007;84:1–15.
[46] Millman J., Halkias C.C. Millman's electronic devices and circuits. 2nd ed., Mc Graw Hill 2007, ISBN: 0070634556.
[47] Hunter Fanney A, Davis MW, Dougherty BP. Comparison of photovoltaic module performance measurements. J Sol Energy Eng Trans ASME 2009;131 (2).
[48] Schroder DK. Semiconductor material and device characterization. New York: John Wiley & Sons, Inc.; 1998.
[49] EES: Engineering Equation Solver. S.A. Klein, Department of Mechanical Engineering, University of Wisconsin-Madison; 〈http://sel.me.wisc.edu/ees/new_ees.html〉.
[50] Villalva M.G., Gazoli J.R., Filho E.R. Modeling and circuit-based simulation of photovoltaic arrays. In: Proceedings of the 10th Brazilian power electronics conference (COBEP); 2009.
[51] Prof. Dr. Marcelo Gradella Villalva. Modeling and simulation of photovoltaic arrays: 〈http://sites.google.com/site/mvillalva/pvmodel〉.
[52] Lo Brano V, Orioli A, Ciulla G. On the experimental validation of an improved five-parameter model for silicon photovoltaic modules. Sol Energy Mater Sol Cells 2012;105:27–39.